Optical absorption enhancement in silicon nanowire arrays with a large lattice constant for photovoltaic applications

Chenxi Lin* and Michelle L. Povinelli

Ming Hsieh Department of Electrical Engineering, University of Southern California, Los Angeles, CA 90089, USA
**chenxil@usc.edu*

Abstract: In this paper, we use the transfer matrix method to calculate the optical absorptance of vertically-aligned silicon nanowire (SiNW) arrays. For fixed filling ratio, significant optical absorption enhancement occurs when the lattice constant is increased from 100nm to 600nm. The enhancement arises from an increase in field concentration within the nanowire as well as excitation of guided resonance modes. We quantify the absorption enhancement in terms of ultimate efficiency. Results show that an optimized SiNW array with lattice constant of 600nm and wire diameter of 540nm has a 72.4% higher ultimate efficiency than a Si thin film of equal thickness. The enhancement effect can be maintained over a large range of incidence angles.

OCIS codes: (310.6628) Subwavelength structures, nanostructures; (350.6050) Solar Energy.

References and links

1. L. Tsakalakos, ""Nanostructures for photovoltaics,"," Mater. Sci. Eng. **62**(6), 175–189 (2008).
2. N. S. Lewis, "Toward cost-effective solar energy use," Science **315**(5813), 798–801 (2007).
3. K. Q. Peng, Y. Xu, Y. Wu, Y. J. Yan, S. T. Lee, and J. Zhu, "Aligned single-crystalline Si nanowire arrays for photovoltaic applications," Small **1**(11), 1062–1067 (2005).
4. L. Tsakalakos, J. Balch, J. Fronheiser, M. Y. Shih, S. F. LeBoeuf, M. Pietrzykowski, P. J. Codella, B. A. Korevaar, O. Sulima, J. Rand, A. Davuluru, and U. Rapol, "Strong broadband optical absorption in silicon nanowire films," J. Nanophotonics **1**(1), 013552 (2007).
5. O. L. Muskens, J. G. Rivas, R. E. Algra, E. P. Bakkers, and A. Lagendijk, "Design of light scattering in nanowire materials for photovoltaic applications," Nano Lett. **8**(9), 2638–2642 (2008).
6. T. Stelzner, M. Pietsch, G. Andra, F. Falk, E. Ose, and S. Christiansen, "Silicon nanowire-based solar cells," Nanotechnology **19**(29), 295203 (2008).
7. V. Sivakov, G. Andrä, A. Gawlik, A. Berger, J. Plentz, F. Falk, and S. H. Christiansen, "Silicon nanowire-based solar cells on glass: synthesis, optical properties, and cell parameters," Nano Lett. **9**(4), 1549–1554 (2009).
8. B. M. Kayes, H. A. Atwater, and N. S. Lewis, "Comparison of the device physics principles of planar and radial p-n junction nanorod solar cells," J. Appl. Phys. **97**(11), 114302 (2005).
9. B. Z. Tian, X. L. Zheng, T. J. Kempa, Y. Fang, N. F. Yu, G. H. Yu, J. L. Huang, and C. M. Lieber, "Coaxial silicon nanowires as solar cells and nanoelectronic power sources," Nature **449**(7164), 885–889 (2007).
10. E. C. Garnett, and P. D. Yang, "Silicon nanowire radial p-n junction solar cells," J. Am. Chem. Soc. **130**(29), 9224–9225 (2008).
11. L. Tsakalakos, J. Balch, J. Fronheiser, B. A. Korevaar, O. Sulima, and J. Rand, "Silicon nanowire solar cells," Appl. Phys. Lett. **91**(23), 233117 (2007).
12. L. Hu, and G. Chen, "Analysis of optical absorption in silicon nanowire arrays for photovoltaic applications," Nano Lett. **7**(11), 3249–3252 (2007).
13. L. J. Lauhon, M. S. Gudiksen, D. Wang, and C. M. Lieber, "Epitaxial core-shell and core-multishell nanowire heterostructures," Nature **420**(6911), 57–61 (2002).
14. M. Law, J. Goldberger, and P. D. Yang, "Semiconductor nanowires and nanotubes," Annu. Rev. Mater. Res. **34**(1), 83–122 (2004).
15. C.-M. Hsu, S. T. Connor, M. X. Tang, and Y. Cui, "Wafer-scale silicon nanopillars and nanocones by Langmuir-Blodgett assembly and etching," Appl. Phys. Lett. **93**(13), 133109 (2008).
16. B. M. Kayes, M. A. Filler, M. C. Putnam, M. D. Kelzenberg, N. S. Lewis, and H. A. Atwater, "Growth of vertically aligned Si wire arrays over large areas (> 1 cm^2) with Au and Cu catalysts," Appl. Phys. Lett. **91**(10), 103110 (2007).

#115811 - $15.00 USD Received 17 Aug 2009; revised 29 Sep 2009; accepted 3 Oct 2009; published 12 Oct 2009

17. J. Zhu, Z. F. Yu, G. F. Burkhard, C. M. Hsu, S. T. Connor, Y. Q. Xu, Q. Wang, M. McGehee, S. H. Fan, and Y. Cui, "Optical absorption enhancement in amorphous silicon nanowire and nanocone arrays," Nano Lett. **9**(1), 279–282 (2009).
18. A. Chutinan, and S. John, "Light trapping and absorption optimization in certain thin-film photonic crystal architectures," Phys. Rev. A **78**(2), 023825 (2008).
19. J. R. Tumbleston, D.-H. Ko, E. T. Samulski, and R. Lopez, "Absorption and quasiguided mode analysis of organic solar cells with photonic crystal photoactive layers," Opt. Express **17**(9), 7670–7681 (2009).
20. D. Duché, L. Escoubas, J.-J. Simon, P. Torchio, W. Vervisch, and F. Flory, "Slow Bloch modes for enhancing the absorption of light in thin films for photovoltaic cells," Appl. Phys. Lett. **92**(19), 193310–193313 (2008).
21. L. Cao, J. S. White, J.-S. Park, J. A. Schuller, B. M. Clemens, and M. L. Brongersma, "Engineering light absorption in semiconductor nanowire devices," Nat. Mater. **8**(8), 643–647 (2009).
22. M. Agrawal and P. Peumans, "Light trapping in solar cells in the wave domain," In preparation.
23. S. H. Fan, and J. D. Joannopoulos, "Analysis of guided resonances in photonic crystal slabs," Phys. Rev. B Condens. Matter **65**(23), 235112 (2002).
24. S. G. Tikhodeev, A. L. Yablonskii, E. A. Muljarov, N. A. Gippius, and T. Ishihara, "Quasiguided modes and optical properties of photonic crystal slabs," Phys. Rev. B Condens. Matter **66**(4), 045102 (2002).
25. T. Prasad, V. L. Colvin, and D. M. Mittleman, "Dependence of guided resonances on the structural parameters of terahertz photonic crystal slabs," J. Appl. Phys. **25**, 633–644 (2008).
26. J. B. Pendry, "Photonic band structures," J. Mod. Opt. **41**(2), 209–229 (1994).
27. D. M. Whittaker, and I. S. Culshaw, "Scattering-matrix treatment of patterned multilayer photonic structures," Phys. Rev. B Condens. Matter **60**(4), 2610–2618 (1999).
28. K. Yamamoto, M. Yoshimi, Y. Tawada, Y. Okamoto, A. Nakajima, and S. Igari, "Thin-film poly-Si solar cells on glass substrate fabricated at low temperature," Appl. Phys., A Mater. Sci. Process. **69**(2), 179–185 (1999).
29. D. F. Edwards, "Silicon (Si)," in *Handbook of optical constants of solids*, E.D.Palik, ed. (Academic, Orlando, Fla., 1985).
30. ASTM, "Reference Solar Spectral Irradiance: Air Mass 1.5 Spectra," *http://rredc.nreal.gov/solar/spectra/am1.5*.
31. M. Li, Z. Y. Li, K. M. Ho, J. R. Cao, and M. Miyawaki, "High-efficiency calculations for three-dimensional photonic crystal cavities," Opt. Lett. **31**(2), 262–264 (2006).
32. M. Li, X. Hu, Z. Ye, K. M. Ho, J. Cao, and M. Miyawaki, "Higher-order incidence transfer matrix method used in three-dimensional photonic crystal coupled-resonator array simulation," Opt. Lett. **31**(23), 3498–3500 (2006).
33. A. Taflove, and S. C. Hagness, *Computational Electrodynamics: The Finite-Difference Time-Domain Method* (Artech, Norwood, MA, 2000).
34. A. Farjadpour, D. Roundy, A. Rodriguez, M. Ibanescu, P. Bermel, J. D. Joannopoulos, S. G. Johnson, and G. W. Burr, "Improving accuracy by subpixel smoothing in the finite-difference time domain," Opt. Lett. **31**(20), 2972–2974 (2006).
35. W. Shockley, and H. J. Queisser, "Detailed balance limit of efficiency of p-n junction solar cells," J. Appl. Phys. **32**(3), 510–519 (1961).
36. J. D. Joannopoulos, R. D. Meade, and J. N. Winn, *Photonic crystals: molding the flow of light*. (Princeton University Press, 2008), Chap. 8.
37. H. R. Philipp, "Silicon Nitride (Si_3N_4)," in *Handbook of optical constants of solids*, E. D. Palik, ed., (Academic, Orlando, Fla., 1985).
38. K. E. Plass, M. A. Filler, J. M. Spurgeon, B. M. Kayes, S. Maldonado, B. S. Brunschwig, H. A. Atwater, and N. S. Lewis, "Flexible Polymer-Embedded Si Wire Arrays," Adv. Mater. **21**(3), 325–328 (2009).
39. J. M. Spurgeon, K. E. Plass, B. M. Kayes, B. S. Brunschwig, H. A. Atwater, and N. S. Lewis, "Repeated epitaxial growth and transfer of arrays of patterned, vertically aligned, crystalline Si wires from a single Si(111) substrate," Appl. Phys. Lett. **93**(3), 032112–032113 (2008).
40. J. Li, H. Yu, S. M. Wong, G. Zhang, X. Sun, P. G.-Q. Lo, and D.-L. Kwong, "Si nanopillar array optimization on Si thin films for solar energy harvesting," Appl. Phys. Lett. **95**(3), 033102–033103 (2009).
41. M. Ghebrebrhan, P. Bermel, Y. Avniel, J. D. Joannopoulos, and S. G. Johnson, "Global optimization of silicon photovoltaic cell front coatings," Opt. Express **17**(9), 7505–7518 (2009).
42. L. Zeng, Y. Yi, C. Hong, J. Liu, N. Feng, X. Duan, L. C. Kimerling, and B. A. Alamariu, "Efficiency enhancement in Si solar cells by textured photonic crystal back reflector," Appl. Phys. Lett. **89**(11), 111111 (2006).
43. P. Bermel, C. Luo, L. Zeng, L. C. Kimerling, and J. D. Joannopoulos, "Improving thin-film crystalline silicon solar cell efficiencies with photonic crystals," Opt. Express **15**(25), 16986–17000 (2007).
44. D. Zhou, and R. Biswas, "Photonic crystal enhanced light-trapping in thin film solar cells," J. Appl. Phys. **103**(9), 093102 (2008).
45. L. Zeng, P. Bermel, Y. Yi, B. A. Alamariu, K. A. Broderick, J. Liu, C. Hong, X. Duan, J. Joannopoulos, and L. C. Kimerling, "Demonstration of enhanced absorption in thin film Si solar cells with textured photonic crystal back reflector," Appl. Phys. Lett. **93**(22), 221105 (2008).
46. S. Pillai, K. R. Catchpole, T. Trupke, and M. A. Green, "Surface plasmon enhanced silicon solar cells," J. Appl. Phys. **101**(9), 093105 (2007).
47. D. M. Schaadt, B. Feng, and E. T. Yu, "Enhanced semiconductor optical absorption via surface plasmon excitation in metal nanoparticles," Appl. Phys. Lett. **86**(6), 063106 (2005).

#115811 - $15.00 USD Received 17 Aug 2009; revised 29 Sep 2009; accepted 3 Oct 2009; published 12 Oct 2009

48. K. R. Catchpole, and A. Polman, "Design principles for particle plasmon enhanced solar cells," Appl. Phys. Lett. **93**(19), 191113 (2008).
49. O. L. Muskens, S. L. Diedenhofen, B. C. Kaas, R. E. Algra, E. P. Bakkers, J. Gomez. Rivas, and A. Lagendijk, "Large photonic strength of highly tunable resonant nanowire materials," Nano Lett. **9**(3), 930–934 (2009).

1. Introduction

Semiconductor nanostructures are promising building blocks for next generation solar cells with higher energy conversion efficiencies and lower cost [1,2]. Silicon-based nanostructured solar cells have several advantages, including the natural abundance of silicon, lack of toxicity, and compatibility with mature integrated-circuit fabrication techniques. Vertically-aligned silicon nanowire arrays exhibit low reflection and strong broadband absorption [3–5] and may be used as antireflection coatings or as the active layer in solar cells [3,6,7]. In particular, silicon nanowire arrays incorporating radial p-n junctions provide advantageous optoelectronic properties [8,9] that relax silicon quality requirement, enabling lower-cost cells. Several groups have demonstrated solar cells based on radial p-n junction SiNW arrays on different substrates [10,11], including silicon wafer and flexible metal foil. Theoretical understanding of optical absorption within SiNW arrays will be critical to guiding further solar cell development.

Optical properties of SiNW arrays over the solar spectrum have previously been calculated by Hu and Chen [12]. They studied arrays with varying nanowire diameters for a fixed lattice constant of 100nm, typical of the structures reported, for example, in Refs [13,14]. Their results showed that SiNW arrays can have much lower reflectance than silicon thin films. However, the overall absorption efficiencies of SiNW arrays were inferior to a silicon thin film of the same thickness. Recently however, fabrication of Si nanowire or microwire arrays with much larger lattice constants (several hundred nanometers to several microns) has been successfully demonstrated [15–17]. In order to design optimal solar cells based on such large-lattice-constant structures, theoretical investigation of their optical properties is needed. In particular, it is of interest to understand the role of optical guided modes in engineering absorption enhancement [18–22]. Guided resonance modes, also known as slow Bloch modes [20], have been extensively studied in photonic-crystal slabs [23–25]. Guided resonance modes are characterized by an increase in electromagnetic field intensity within the photonic-crystal slab, which results from the coupling of incident light from air to high-Q leaky modes of the 2D periodic structure [23–25]. Therefore, it is expected that when guided resonance modes are excited by incident sunlight, the optical absorption will be strongly enhanced.

In this paper, we use the transfer matrix method (TMM) [26,27] to calculate the optical properties of SiNW arrays with lattice constants between 100 and 600nm. We show that for fixed filling ratio (defined as $\pi d^2/4a^2$, where d is the nanowire diameter and a is the lattice constant), increasing the lattice constant of the SiNW array yields dramatic optical absorption enhancement in the low-frequency range of the solar spectrum. For proper choice of lattice constant and filling ratio, we find that the overall absorption efficiency of SiNW arrays can surpass that of a Si thin film of equal thickness and even that of an equal-thickness Si thin film with an optimal single-layer AR coating. For lattice constants below ~250nm, guided resonance modes are not present. The absorption efficiency increases with lattice constant due to a greater concentration of fields within the dielectric material. Above ~250nm, the presence of guided resonance modes further increases absorption efficiency. We optimize the optical absorption with respect to lattice constant and filling ratio and calculate the dependence of absorption efficiency on incidence angle for the optimal structure.

2. Methods

Figure 1(a) illustrates the vertically aligned SiNW array structure we study. The SiNW array is illuminated from the top by sunlight, in the direction indicated by the red arrow. The electric field of the incident light is polarized along the x-axis. The array consists of silicon nanowires with diameter d and period a arranged in a square lattice and surrounded by air. In

#115811 - $15.00 USD Received 17 Aug 2009; revised 29 Sep 2009; accepted 3 Oct 2009; published 12 Oct 2009

our calculations, we fixed the nanowire length L to 2.33μm. This value is comparable to the film thickness in silicon thin film solar cells [28] and allows us to compare our results to those in Ref [12]. The lattice constant a was varied from 100nm to 600nm. The filling ratio was varied from 0.2 to 0.79; for a filling ration of 0.79, the nanowire diameter is equal to the lattice constant. Figure 2(a) shows the frequency-dependent refractive index and absorption length of crystalline silicon, taken from Ref [29]. We assume that the nanowires are lightly doped, so that both n-type and p-type regions can be modeled using the same refractive index and absorption length as intrinsic crystalline silicon. In Fig. 2(b), we plot the ASTM Air Mass 1.5 direct and circumsolar solar spectrum [30]. For solar cell applications, the frequency range of interest is 1.1eV – 4eV, from the band gap edge of crystalline silicon (1.1eV) to where the solar spectral irradiance is negligibly small.

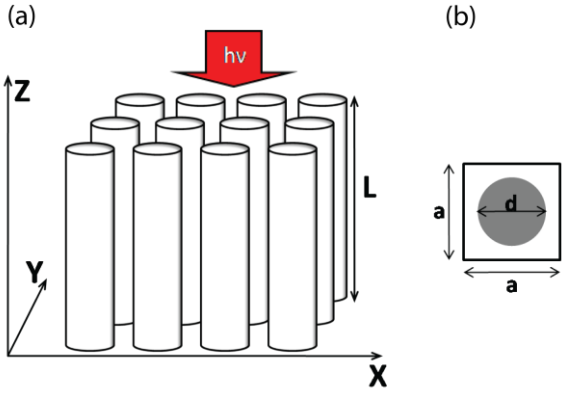

Fig. 1. (a) Schematic of the vertically aligned silicon nanowire array. (b) Cross-sectional view of a single silicon nanowire.

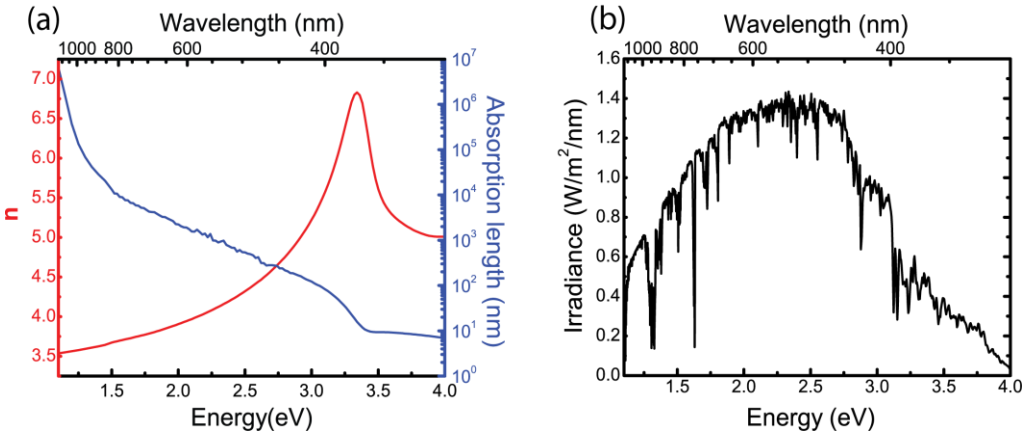

Fig. 2. (a) Refractive index (left axis) and absorption length (right axis) of crystalline silicon from Ref [29]. (b) The ASTM Air Mass 1.5 direct and circumsolar solar spectrum from Ref [30].

#115811 - $15.00 USD Received 17 Aug 2009; revised 29 Sep 2009; accepted 3 Oct 2009; published 12 Oct 2009

We use the transfer matrix method (TMM) to calculate the reflectance, transmittance, and absorptance of SiNW arrays. The transfer matrix method is an efficient frequency-domain method for dealing with periodic structures. We use the freely available ISU-TMM simulation package for our study [31,32] that can determine the frequency-dependent reflectance $R(\omega)$ and transmittance $T(\omega)$ from the scattering matrix of the nanowire structure. The absorptance is calculated as $A(\omega) = 1\text{-}R(\omega)\text{-}T(\omega)$. Calculations were carried out on a PC equipped with a single Intel Core 2 Quad 2.66GHz processor. Calculation times for a single frequency point ranged from less than one second for the smallest lattice constant to more than two minutes for the largest lattice constant under study.

We also use the finite-difference time-domain method [33] to calculate the electromagnetic field distributions inside the SiNW arrays as well as the dispersive band structure. We use the freely available MEEP software package [34] for calculating the field distribution and Lumerical FDTD solutions simulation package for calculating the dispersive band structure.

In order to quantify the absorption of different SiNW arrays across the solar spectrum, we calculate the ultimate efficiency [35]. The ultimate efficiency is defined by the assumption that each absorbed photon with energy greater than the band gap produces one and only one electron-hole pair with energy hc/λg, where λg is the wavelength corresponding to the band gap of Si. It is given by

$$\eta = \frac{\int_{310nm}^{\lambda_g} I(\lambda)A(\lambda)\frac{\lambda}{\lambda_g}\,d\lambda}{\int_{310nm}^{4000nm} I(\lambda)d\lambda}$$

where λ is wavelength, $I(\lambda)$ is the spectral irradiance (power density) of the ASTM AM1.5 direct normal and circumsolar spectrum, $A(\lambda)$ is the absorptance, and λ_g = 1127nm is the wavelength corresponding to the 1.1eV band gap of crystalline silicon. The lower limit of the integral, 310nm, corresponds to an energy E = 4eV, and the upper limit of the integral in the denominator, 4000nm, is the upper limit of the available data for the solar spectrum. The integrals were evaluated using the trapezoid rule with 908 sampling points.

The ultimate efficiency can be related to the maximum short circuit current by assuming perfect carrier collection efficiency, i.e., every photogenerated carrier can reach the electrodes and contribute to the photocurrent. In this case,

$$J_{sc} = \int_{310nm}^{\lambda_g} I(\lambda)A(\lambda)\frac{e\lambda}{hc}\,d\lambda = \eta \times \frac{e\lambda_g}{hc} \times \int_{310nm}^{4000nm} I(\lambda)d\lambda = 81.83\eta\left(mA/cm^2\right)$$

3. Results and Discussion

We expect that excitation of guided resonance modes will lead to strong interaction between incident light and the SiNW array, exhibiting itself as an increase in absorption. However, guided resonances will only be present at frequencies within the solar spectrum when the lattice constant is sufficiently large, as pointed out in Ref [20]. in the context of organic solar cells. We illustrate the effect of changing the lattice constant in Fig. 3(a) and (b), where the dispersive band structures of a = 100nm and a = 500nm SiNW arrays are shown side by side. We plot both Z-even (TE-like) and Z-odd (TM-like) modes [36]. Guided resonance modes lie within the shaded region, called the light cone. The figure shows that for energies up to 2.8eV, guided resonance modes are not present for the a = 100nm SiNW array. For the a = 500nm SiNW array, guided resonance modes appear at energies of 0.97eV and above. Modes at the Γ point can be excited by normal incident sunlight.

#115811 - $15.00 USD Received 17 Aug 2009; revised 29 Sep 2009; accepted 3 Oct 2009; published 12 Oct 2009

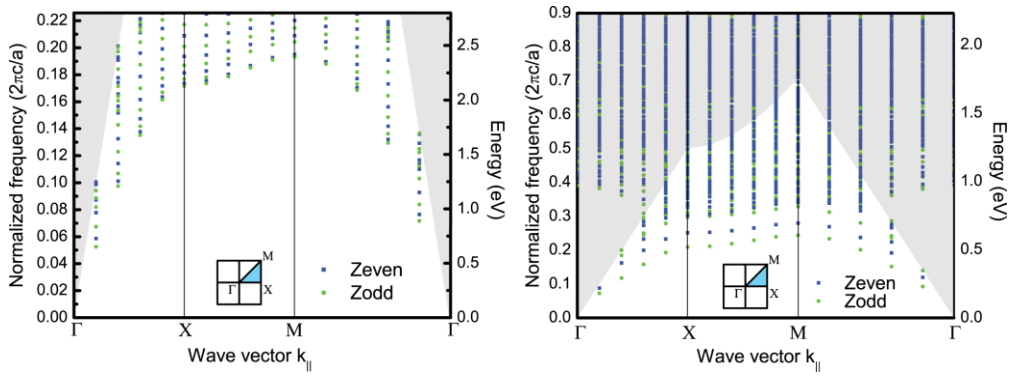

Fig. 3. The dispersive band structures of a SiNW array for (a) a = 100nm (b) a = 500nm.

Figures 4(a), (b), and (c) compare the reflectance, transmittance, and absorptance of arrays with a = 100nm and a = 500nm for a fixed filling ratio of 0.28. Data for a thin film are shown for comparison. The results for the SiNW array with lattice constant a = 100nm agree well with previous study [12]. The reflectance (R) in Fig. 4(a) is much lower than that of the thin film throughout the entire spectral range. Meanwhile, the transmittance (T) in Fig. 3(b) is much higher than the Si thin film in the low-frequency range and approaches zero in the high-frequency range. The absorptance, shown in Fig. 4(c), is given by $A = 1-R-T$. In the high-frequency range, the low reflectance and zero transmittance of the SiNW array lead to higher absorptance than the Si thin film. In the low-frequency range, the SiNW array has a lower absorptance than the thin film. We calculated the ultimate efficiency for both structures and found that the efficiency of the thin film (13.83%) is higher than that of the SiNW array (7.62%). We note that these values are close but not identical to those given in Ref [12]; slight differences may be due to the use of different optical constant data near the band gap or to differences in implementation of the TMM method. We have verified that the ultimate efficiency of the thin film calculated using the TMM code agrees with that calculated using the analytical formula for the transmittance and reflectance of a lossy slab within 0.3%.

For a = 500nm, narrow, irregularly-spaced peaks appear in the reflectance spectrum (Fig. 4(a)) that are qualitatively different than the Fabry-Perot-like features seen in the thin film and a = 100nm lattice constant SiNW structures in the low frequency range. The transmittance spectrum (Fig. 4(b)) exhibits narrow dips, and the absorptance spectrum (Fig. 4(c)) exhibits numerous enhancement peaks. In the high-frequency range, narrow spectral features are largely absent in the reflectance, transmittance, and absorptance data. This phenomenon can be explained by the high material absorption of Si in this range (Fig. 2(a)). We have observed in numerical experiments that increasing the absorption of the nanowire material tends to smooth out guided resonance peaks.

#115811 - $15.00 USD Received 17 Aug 2009; revised 29 Sep 2009; accepted 3 Oct 2009; published 12 Oct 2009

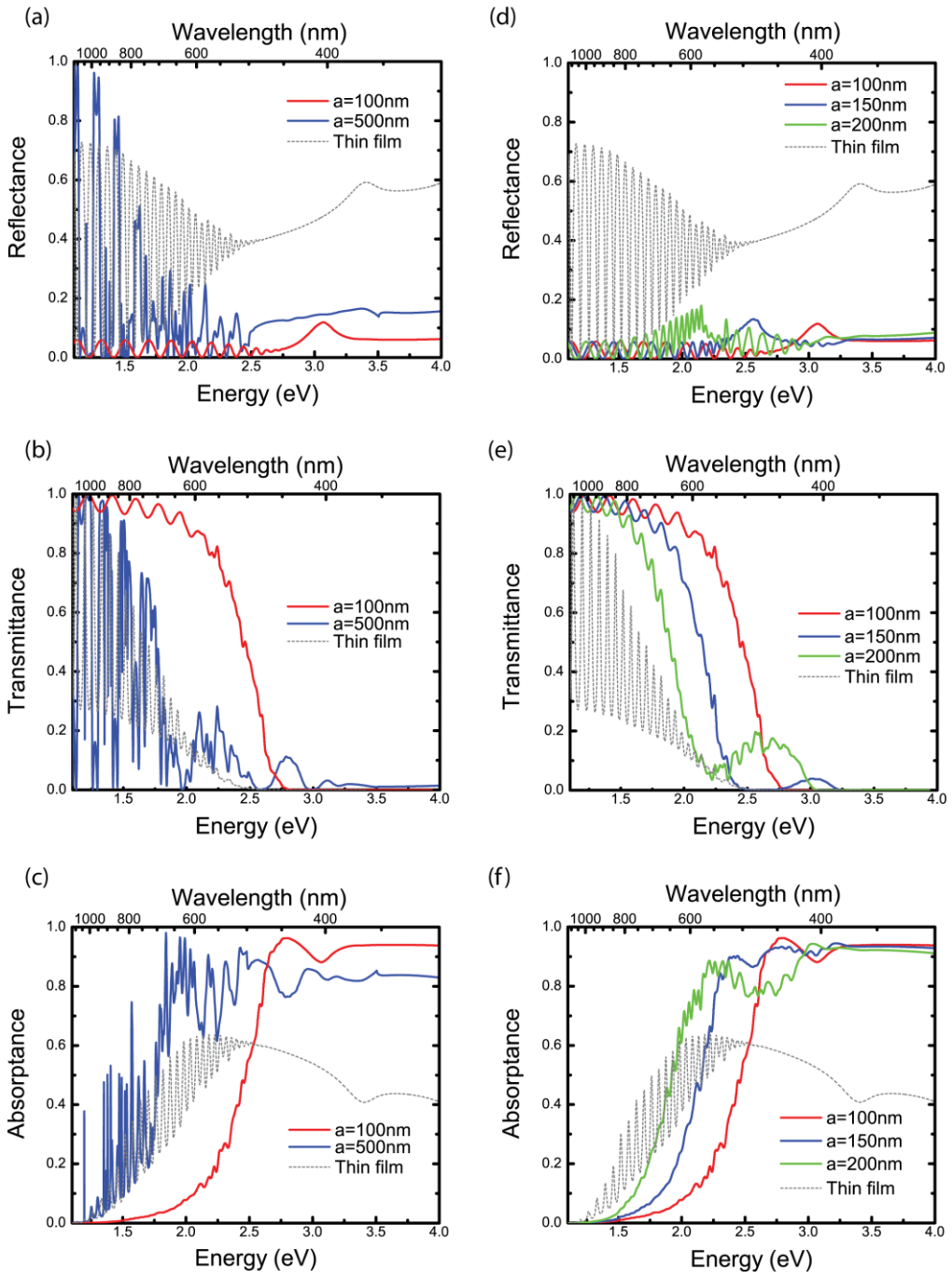

Fig. 4. Optical properties of the SiNW array with varying lattice constant. In the left column, (a), (b), and (c) are the reflectance, transmittance, and absorptance, respectively, in the SiNW array with lattice constant 100nm and 500nm. The optical properties of a silicon thin film are plotted for comparison. In the right column, (d), (e), and (f) are the reflectance, transmittance, and absorptance, respectively, in the SiNW array with lattice constants 100nm, 150nm, and 200nm. The optical properties of the Si thin film are also plotted.

In Fig. 5(a), we show the reflectance, transmittance, and absorptance data for the a = 500nm SiNW array in a narrow spectral region around 1.197eV. A transmittance dip is

#115811 - $15.00 USD Received 17 Aug 2009; revised 29 Sep 2009; accepted 3 Oct 2009; published 12 Oct 2009

accompanied by a reflectance peak. The absorptance exhibits an enhancement peak, consistent with a relative increase in electromagnetic field intensity at the resonant frequency. The electric field density distributions ($\varepsilon|E|^2$) on the end surface of the SiNW and on a vertical cross section of the nanowire structure are shown in Figs. 5(b) and (c). The field density is concentrated in the absorptive SiNW region.

We calculated the ultimate efficiency for the a = 500nm array and found a value of 20.67%, higher than the thin film of equal thickness (13.83%). Thus we find that for a suitably chosen lattice constant and filling fraction, the absorptivity of the SiNW array is in fact higher than for a solid film.

Referring back to Fig. 4(c), an additional difference between the a = 100nm and a = 500nm data is visible. In addition to the presence of guided resonance peaks, the overall shape of the a = 500nm curve is shifted toward lower energies than the a = 100nm curve. In order to understand this trend, we plot the optical properties of SiNW arrays with intermediate lattice constants for which guided resonance modes are not present.

Figures 4(d), (e), and (f) show the results for a = 100nm, 150nm, and 200nm. For a = 150nm and 200nm, the reflectance values in Fig. 4(d) remain low across the entire spectral range. The transmittance curve, shown in Fig. 4(e), tends to shift towards lower energies (higher wavelengths) as the lattice constant is increased. The transmittance in the high-frequency range is close to zero for all three lattice constants. The absorptance curves (Fig. 4(f)) also shift to lower energies, while the absorptance is high in the high-frequency range for all three lattice constants. We calculated ultimate efficiencies of 7.62%, 12.34%, and 16.14% for the SiNW arrays with lattice constants a = 100nm, 150nm, and 200nm, respectively, compared to 13.83% for the Si thin film of equal thickness. The increase in absorptance with increasing lattice constant (even in the absence of guided resonances) can be understood in terms of the field concentration inside the silicon nanowires. We have verified via FDTD simulations that for fixed filling ratio, the normalized electromagnetic field energy inside the silicon nanowire increases with increasing lattice constant.

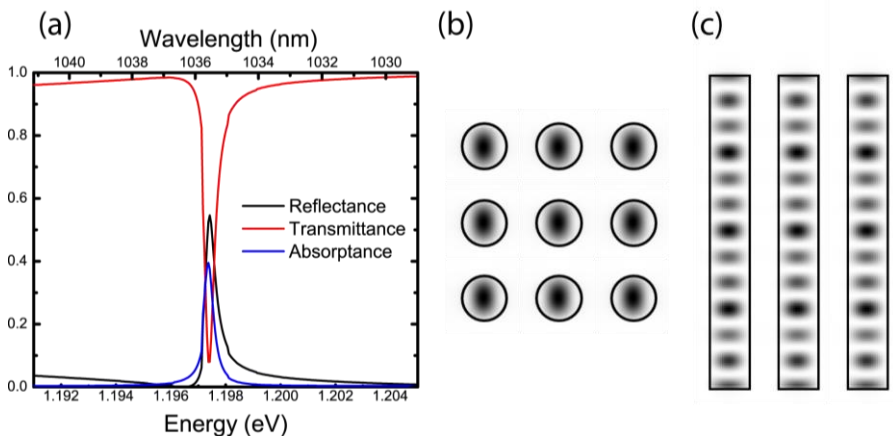

Fig. 5. (a) Characteristic line shape of a guided resonance at 1.197eV (b) Top view of electric field energy density distribution on the end surface of the SiNW array at the resonance shown in (a). (c) Side view of electric field energy density distribution inside the nanowires at the same resonance.

#115811 - $15.00 USD Received 17 Aug 2009; revised 29 Sep 2009; accepted 3 Oct 2009; published 12 Oct 2009

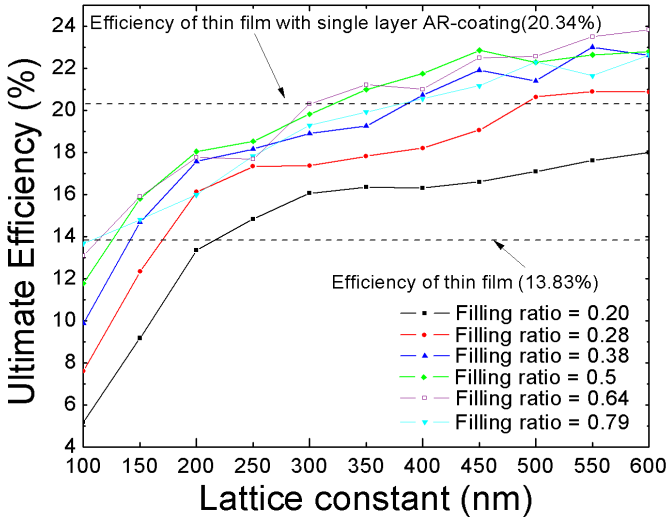

Fig. 6. Ultimate efficiency of the SiNW array as a function of lattice constant for several filling ratios.

Figure 6 shows the dependence of the ultimate efficiency on the lattice constant and filling ratio. For fixed filling ratio, the ultimate efficiency tends to increase with increasing lattice constant. This trend arises from enhanced field concentration within the rods and the excitation of guided resonances, as discussed above. For fixed lattice constant, the ultimate efficiency initially increases with filling ratio but then decreases again. This trend can be explained by the fact that as the filling ratio approaches one, the efficiency of the nanowire array should approach that of a thin film (lower dashed line). From the graph, the optimal range of the filling ratio is between 0.5 and 0.64.

It is clear from the graph that the ultimate efficiency of a SiNW array with lattice constant larger than 150nm can exceed that of an equally-thick Si thin film (lower dashed line), given proper choice of filling fraction. Moreover, a SiNW array with lattice constant larger than 350nm can exceed that of Si film with a single layer antireflection (AR) coating (upper dashed line). We calculated the efficiency of the AR-coated thin film assuming a single-layer coating of silicon nitride (Si_3N_4) with frequency-dependent refractive index given in Ref [37]. In the frequency range of interest, Si3N4 has negligible loss. We optimized the thickness of the AR-coating to maximize the efficiency, yielding an efficiency of 20.34% at a thickness of 63nm. Within the parameter range shown in Fig. 6, the optimal SiNW structure has a lattice constant of 600nm and a diameter of 540nm. It can achieve an ultimate efficiency of 23.84%, 72.4% higher than the efficiency of a Si thin film of equal thickness and 17.2% higher than an equal-thickness Si thin film with an optimal single-layer AR coating.

#115811 - $15.00 USD Received 17 Aug 2009; revised 29 Sep 2009; accepted 3 Oct 2009; published 12 Oct 2009

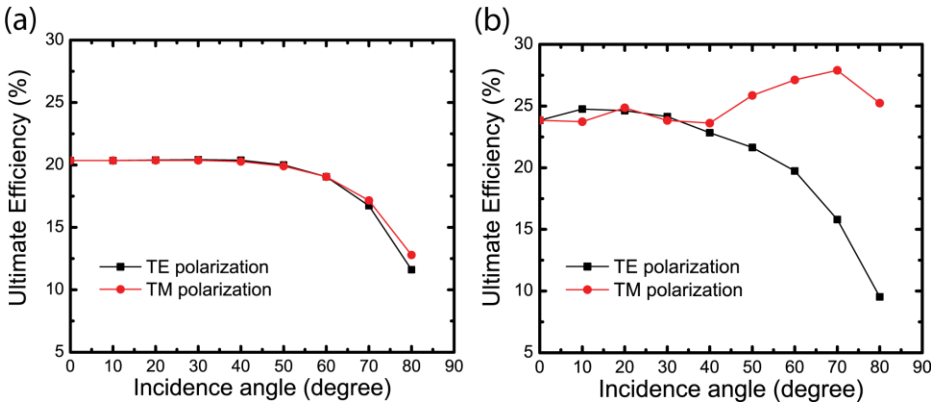

Fig. 7. The dependence of ultimate efficiency on incidence angle for (a) a 2.33μm-thick Si thin film with an optimized single-layer antireflection coating and (b) an optimal SiNW array (a = 600nm, d = 540nm).

In Fig. 7(a), we show the ultimate efficiency as a function of incidence angle for the optimal SiNW array (a = 600nm, d = 540nm). For comparison, we plot the ultimate efficiency for a Si thin film with optimized single-layer AR coating (Fig. 7(b)). The efficiency of the SiNW array tends to be higher for TM polarized light than for TE polarized light. In comparison to the AR-coated Si thin film, the SiNW array is more absorptive to TM-polarized light for angles up to 80 degrees and more absorptive to TE-polarized light for angles up to 60 degrees. Detailed calculations showed that the difference in ultimate efficiency between TE and TM polarizations for the SiNW array may be attributed to higher reflectance of TM-polarized light in the high-frequency range. TE reflectance increases with incidence angle in the high-frequency range, while TM reflectance decreases.

4. Conclusion

In conclusion, we use the transfer matrix method to study the optical properties of SiNW arrays with lattice constants varying from 100nm to 600nm. Our results show that dramatic optical absorption enhancement occurs with increasing lattice constant. For relatively small lattice constants, the absorption enhancement results from an increase in the electromagnetic field concentration within the silicon nanowires. For larger lattice constants, guided resonances are excited and serve as a supplemental enhancement mechanism. We demonstrate that by tuning the lattice constant and the filling ratio, a SiNW array can be found that is more absorptive than an equally-thick Si thin film with a single-layer antireflection coating. The optimal SiNW array has a lattice constant of 600nm and a filling ratio of 0.79, and it exhibits an ultimate efficiency of 23.84%. The optical absorption enhancement effect is maintained over a large range of incidence angles.

In this paper, we focus on SiNW arrays with symmetry in the vertical direction. Such arrays have been fabricated and embedded in low-index polymers [38,39]. The arrays can be transferred onto flexible substrates. Our work will be of direct relevance to such systems.

Alternatively, other work in the literature has studied SiNW arrays on top of silicon substrates. Experimentally, it has been observed that the absorption of such a composite structure can exceed that of a thin film [4]. Similarly, a very recently published modeling paper [40] has shown that the ultimate efficiency of a composite system can surpass that of a thicker silicon film. In that work, the role of guided resonances was not explicitly identified. Untangling the contributions of guided resonance modes from the effects of Fabry-Perot resonance modes in the substrate, as well as the effects of increased field concentration in the dielectric with increasing lattice constant, is a challenging task that will require further research.

#115811 - $15.00 USD Received 17 Aug 2009; revised 29 Sep 2009; accepted 3 Oct 2009; published 12 Oct 2009

In future work, it will also be interesting to determine whether further absorption enhancement can be obtained in SiNW arrays by using antireflection coatings [41], photonic-crystal back reflectors [42–45], or plasmonic excitation [4,46–48]. The properties of microwire arrays, with even larger lattice constants and nanowire diameters than those studied here, are also an intriguing area of study. In all of these cases, untangling the rich optical mode structure of the patterned solar cell material will be important for understanding the ultimate limits of engineered absorption enhancement. Likewise, the effect of randomness and disorder [49] in increasing or decreasing the ultimate efficiency of nanowire arrays is an important area for further research.

Acknowledgements

Chenxi Lin is funded by a USC Provost's Fellowship. Michelle Povinelli is funded through USC Powell and WiSE Jr. Gabilan faculty awards. The authors thank Dr. Ming Li for providing the ISU-TMM photonic crystal simulation package. Computing resources were provided by the USC Center for High Performance Computing and Communications.

#115811 - $15.00 USD Received 17 Aug 2009; revised 29 Sep 2009; accepted 3 Oct 2009; published 12 Oct 2009